Ab initio study of point defects in magnesium oxide

C. A. Gilbert, S. D. Kenny,* R. Smith, and E. Sanville

Department of Mathematical Sciences, Loughborough University, Loughborough LE11 3TU, United Kingdom
(Received 4 May 2007; revised manuscript received 25 July 2007; published 6 November 2007)

Energetics of a variety of point defects in MgO have been considered from an *ab initio* perspective using density functional theory. The considered defects are isolated Schottky and Frenkel defects and interstitial pairs, along with a number of Schottky defects and di-interstitials. Comparisons were made between the density functional theory results and results obtained from empirical potential simulations and these generally showed good agreement. Both methodologies predicted the first nearest neighbor Schottky defects to be the most energetically favorable of the considered Schottky defects and that the first, second, and fifth nearest neighbor di-interstitials were of similar energy and were favored over the other di-interstitial configurations. Relaxed structures of the defects were analyzed, which showed that empirical potential simulations were accurately predicting the displacements of atoms surrounding di-interstitials, but were overestimating O atom displacement for Schottky defects. Transition barriers were computed for the defects using the nudged elastic band method. Vacancies and Schottky defects were found to have relatively high energy barriers, the majority of which were over 2 eV, in agreement with conclusions reached using empirical potentials. The lowest barriers for di-interstitial transitions were found to be for migration into a first nearest neighbor configuration. Charges were calculated using a Bader analysis and this found negligible charge transfer during the defect transitions and only small changes in the charges on atoms surrounding defects, indicating why fixed charge models work as well as they do.

I. INTRODUCTION

In recent years, computer simulations that predict the behavior of materials are becoming more and more sophisticated and therefore useful. Modeling the effects of radiation damage in oxide materials is one such area of study that has been receiving a lot of attention, due to the fact that there is an increasing interest in storing radioactive waste safely for long periods of time. It is therefore important to be able to predict accurately the behavior of the affected materials over long time scales. Materials that have come under scrutiny in the past are ceramics based on the MgO-Al_2O_3 system, the simplest of which is magnesium oxide (MgO).

MgO has a relatively simple crystal structure, known as the NaCl (or rocksalt) structure, and this is one of the reasons that make this oxide such an appealing material to consider. Its simplicity and well understood properties have resulted in MgO being utilized as a test material for both experimental analysis and computer simulation. There are well established empirical potentials existing for MgO and these have given rise to detailed molecular dynamics studies[1–6] of various properties of the material.

Simulations that utilize empirical potentials are extremely useful as they can be used to describe the defects in the material that would result from exposure to radiation. It was shown previously[2,3] that the main types of defect present after a collision cascade in MgO were Frenkel defects, Schottky defects, and di-interstitials. It is due to this observation that the study in this paper considers these specific defects.

The empirical potential model itself, although successful, is still not necessarily creating the most accurate picture of the defect energetics. It is therefore of interest to study these defects from a more accurate *ab initio* perspective. The energetics of a Schottky defect in MgO have already been studied using a Hartree-Fock cluster embedded within a crystal by Grimes *et al.*,[7] and the energy was found to be 8.2 eV. Isolated Schottky defects were studied using density functional theory (DFT) by De Vita *et al.*[8,9] Their result using quite a small supercell containing 32 atoms shows a prediction of a formation energy lying in the region between 6 and 7 eV. A more recent DFT calculation was performed by Alfe and Gillan[10] in which they found the formation energy of an isolated Schottky defect to be 6.99 eV.

In this paper, these isolated defects have also been studied, but using a much larger supercell allowing the calculation of accurate formation energies. We have also considered not only isolated defects but also interacting defects in the form of Schottky defects and di-interstitials. Furthermore, we have studied a number of energy barriers involving the migration and transformation of these defects.

II. METHODOLOGY

The main body of work carried out in this paper has been performed using the *ab initio* code PLATO (package for linear combination of atomic-type orbitals).[11] This code utilizes density functional theory[12,13] using localized, numerical orbitals. Pseudopotentials for magnesium and oxygen were taken from the work of Hartwigsen *et al.*[14] and it is important to note that a semicore pseudopotential was used for Mg. The local density approximation[15] was used to describe exchange correlation within the system as this has been shown to give good agreement with experiment for MgO (Refs. 8 and 9) and with higher order methods.[10] Our basis sets contained 23 basis functions for Mg and 14 basis functions for O. The required numerical integrations were carried out on an atom centered grid consisting of 40 points in the radial

direction and 35 points in the angular direction.

Tests were carried out upon the convergence of the equilibrium lattice constant and bulk modulus of MgO with a variety of Monkhorst-Pack[16] **k**-point mesh sizes. A $6 \times 6 \times 6$ mesh was settled upon (for the eight atom cubic unit cell) as this provided sufficiently converged values for both the bulk parameters and the total energy of the eight atom cell. For larger cells, equivalent meshes were used. The resulting lattice constant was predicted to be 4.17 Å and the bulk modulus was 1.65 Mbar. De Vita *et al.*[8,9] computed an identical prediction for the lattice constant with a slightly lower bulk modulus of 1.54 Mbar using a plane wave basis set, indicating that our localized orbital basis set is performing well for bulk systems. These values compare well with the experimental parameters, which are 4.21 Å (Ref. 17) for the lattice constant and 1.55 Mbar (Ref. 18) for the bulk modulus of MgO.

For the isolated defects, two additional electrons were added to the system in the case of a Mg vacancy, and two were removed for an O vacancy. Equivalent electron additions and subtractions were made for the isolated interstitials. This is to take into account the ionic nature of the material. Testing was performed by varying this integer number of electrons between 0 and 3, and it was shown that the two electron insertion or removal produces the minimum formation energies.

We have also used an empirical potential approach to calculate the defect energetics. A model without shells, as this is typically used in dynamical simulations, was implemented and the potential used is given in Eq. (1). This is a standard Buckingham potential. The parameters A, C, and ρ are from Lewis and Catlow.[19]

$$\phi(r) = A \exp\left(-\frac{r}{\rho}\right) - \frac{C}{r^6} + V(r). \qquad (1)$$

The most common defects found in empirical potential simulations of collision cascades in MgO are di-interstitials and Schottky defects. Thus, we have calculated the formation energies of these as a function of their separation distances. It was also of interest to calculate the formation energies of isolated Schottky and Frenkel defects and interstitial pairs. The isolated defects allow us to assess when the defect pairs are sufficiently separated such that there is no longer any interaction between the two defects comprising the pair.

For the defect pairs, we have considered three different Schottky defects and five different di-interstitial configurations, all defined by the separation between the two defects in the pair. Schottky defects are formed with the removal of one Mg atom and one O atom from the system, and in a similar way the di-interstitials consist of adding an additional Mg and an additional O to the system. The initial configurations of these defects are shown in Figs. 1 and 2. It is important to note that the distance between the vacancies in a second nearest neighbor Schottky defect configuration is initially the same as the distance between the interstitials in a third nearest neighbor di-interstitial configuration, and the same comparison is true for a third nearest neighbor Schottky defect and a fifth nearest neighbor di-interstitial.
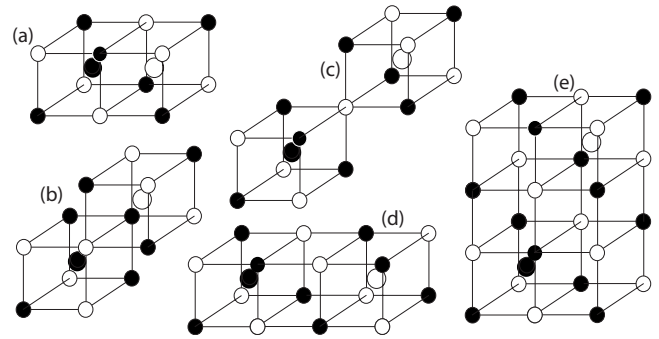

FIG. 1. The initial configurations of atoms for the (a) first, (b) second, (c) third, (d) fourth, and (e) fifth nearest neighbor di-interstitials. The black circles represent the Mg atoms, while the white circles represent the O atoms.

Periodic boundary conditions were utilized in the DFT calculations and so a supercell approach was taken. A relatively small number of atoms were considered and these were effectively repeated throughout space due to the conditions imposed by the boundaries. When doing this, since any defects placed in the supercell are also repeated, it was necessary to create a supercell of suitable size and shape such that the interaction between the defect and its periodic repeats was minimized. We have performed a series of calculations for each defect in which we increased this separation between the defect and the repeats, thus creating a set of formation energies for each defect.

In order to optimize the supercells so that the minimum number of atoms is considered for a specific separation distance, thus increasing computational efficiency, a methodology was implemented that allowed a variety of shapes of supercell to be considered. The computational tool CRYSTAL (Ref. 20) also implements the method. This method utilizes a transformation matrix which repeats the two atom MgO primitive cell to create a larger supercell of the required size and shape. This is carried out by first considering a transformation matrix T, which contains integers t_{ij} for $i,j = 1, \ldots, 3$, and this is used to construct three supercell vectors $(\mathbf{s}_1, \mathbf{s}_2, \mathbf{s}_3)$ from the three primitive cell vectors $(\mathbf{p}_1, \mathbf{p}_2, \mathbf{p}_3)$ as shown in Eq. (2),

$$\mathbf{s}_1 = t_{11}\mathbf{p}_1 + t_{12}\mathbf{p}_2 + t_{13}\mathbf{p}_3,$$
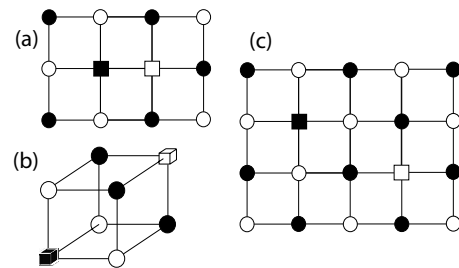

FIG. 2. The initial configurations of the atoms for the (a) first, (b) second, and (c) third nearest neighbor Schottky defects. The circles represent atoms, while the squares represent vacancies. Black squares are Mg vacancies and white squares are O vacancies. This notation is used in all subsequent figures.

TABLE I. The sizes of the supercells used in the simulations of the defects using DFT. The minimum separation distance, in Å, between the periodic repeats of the defects is given in square brackets alongside the number of atoms.

Defect(s)	Number of atoms [Separation distance (Å)]			
	Cell 1	Cell 2	Cell 3	Cell 4
1NN di-interstitial/ 1NN Schottky defect	32 [5.90]	48 [7.52]	90 [8.85]	128 [10.43]
2NN di-interstitial	32 [5.90]	58 [7.80]	84 [8.85]	132[10.22]
3NN di-interstitial/ 2NN Schottky defect	32 [5.90]	56 [7.52]	90 [8.85]	144 [10.43]
4NN di-interstitial	32 [5.90]	54 [6.60]	84 [8.85]	128 [9.33]
5NN di-interstitial/ 3NN Schottky defect	40 [5.90]	64 [7.52]	104 [8.85]	160 [10.43]
Isolated interstitial/vacancy	8 [4.17]	64 [8.34]	128 [11.65]	180 [12.86]

$$s_2 = t_{21}\mathbf{p}_1 + t_{22}\mathbf{p}_2 + t_{23}\mathbf{p}_3,$$

$$s_3 = t_{31}\mathbf{p}_1 + t_{32}\mathbf{p}_2 + t_{33}\mathbf{p}_3. \tag{2}$$

Given a variety of supercells containing the same number of atoms, the most suitable one is that which maximizes the distance between a defect placed within the cell and with its periodic repeat generated through application of periodic boundary conditions. The results of this optimization are shown in Table I. From this, it can be seen that we have maintained approximately the same separation distances for each of the different defect types. Since some of the defects have a larger separation, it is unavoidable that larger super-cells, containing more atoms, are needed to maintain the same separation distance between the defects and their re-peats.

The formation energy of a defect, E_{form}, which is the en-ergy required to form the defect in the perfect crystal struc-ture, is calculated using Eq. (3) for the case of a pair of isolated defects. $E_n(i,j)$ is the total cell energy for a supercell containing n lattice sites with i defects of one species and j defects (of the same type) of the other. In the parentheses, the $\pm$ becomes positive for the case of interstitial defects and becomes negative for the case of vacancies. $E_n(0,0)$ is the perfect lattice energy.

$$E_{form} = E_n(1,0) + E_n(0,1) - 2\left(\frac{n \pm 1}{n}\right)E_n(0,0). \tag{3}$$

A simplified version of this [Eq. (4)] is used for calculating the formation energy of di-interstitials and Schottky defects, where now both interstitials or vacancies are placed within the same supercell and so can interact.

$$E_{form} = E_n(1,1) - \left(\frac{n \pm 2}{n}\right)E_n(0,0). \tag{4}$$

Transition barriers have been calculated by using the nudged elastic band method with a modified tangent approach.[21] We utilized a spring constant of $k = 0.4$ eV/Å^2 to compute the states of the system at 10–12 points (depending on the system size) along the minimum energy path between two local minima. Forces were computed at each step, and atoms were positioned in new locations, until the maximum force was found to be below 0.07 eV/Å. The maximum en-ergy of this minimum energy path (the saddle point) was then found by fitting a cubic spline through the obtained data points, clamped in such a way to force the gradient to be zero at the local minima that represent the relaxed structures. An example of this is shown in Fig. 3.

Charges within the defective systems were computed us-ing a Bader charge analysis with Bader volumes allocated using the methodology found in Ref. 22.

III. RESULTS

A. Defect formation energies and geometrical structure

DFT calculations of the formation energies of isolated Schottky and Frenkel defects and interstitial pairs for the cell sizes presented in Table I give results as shown in Table II.

From the largest cell size for these defects, the formation energy of a pair of isolated vacancies appears to converge to 6.0 eV, whereas for the pair of isolated interstitials, the for-mation energy is 16.6 eV. These results differ by less than
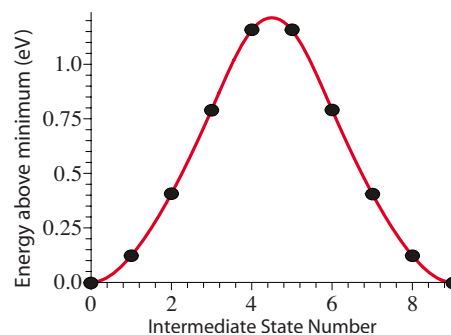

FIG. 3. (Color online) This graph shows how a clamped cubic spline is fitted to a series of calculated energies for the transition of an isolated interstitial in a 54 atom system. The black dots represent the intermediate states between the initial and final system configurations.

TABLE II. The formation energies from the DFT calculations for the pairs of isolated defects as a function of the system size.

Number of atoms	Schottky defect	Isolated interstitial pair	Frenkel defect	
			Magnesium	Oxygen
8	7.23	20.04	13.55	13.72
64	5.65	16.35	10.07	11.93
128	5.88	16.74	10.33	12.31
180	5.97	16.58	10.35	12.17

3 eV from those formation energies predicted by an empirical potential simulation of a cell containing 64 000 atoms, which utilizes the potential stated in Eq. (1). The classical potential predicts formation energies of 8.8 eV for the isolated vacancies and 18.4 eV for isolated interstitials, both of which are overestimates of the energies calculated using DFT. The isolated Mg Frenkel defect has a formation energy of approximately 10.3 eV compared with an empirical potential estimate of 14.1 eV, and for the O Frenkel defect, DFT computes a formation energy of 12.2 eV and the empirical potential simulation predicts 13.6 eV. The energies of the isolated Frenkel defects have also been calculated using the empirical potentials with shells. This gives a formation energy of 12.6 eV for the Mg Frenkel defect and 12.3 eV for the O Frenkel defect.

In addition to calculating the formation energies for these isolated defects, the energetics of di-interstitials and Schottky defects were studied, and in this case interaction is allowed between the two defects comprising the pair. Figure 4 shows how these formation energies converge as the supercells are increased in size to negate any interactions between the defect pairs and the periodic images of the defect pairs (which are introduced by periodic boundary conditions). The defect energies are converged to within ±0.2 eV for sufficiently large supercells.

Table III shows the formation energy for each of these defects taken from the computation for the largest cell for that particular defect. These are compared to the empirical potential simulation predictions for the formation energies for each of the different defects.

From these comparisons, it can be seen that the empirical potential simulations overestimate the formation energies for
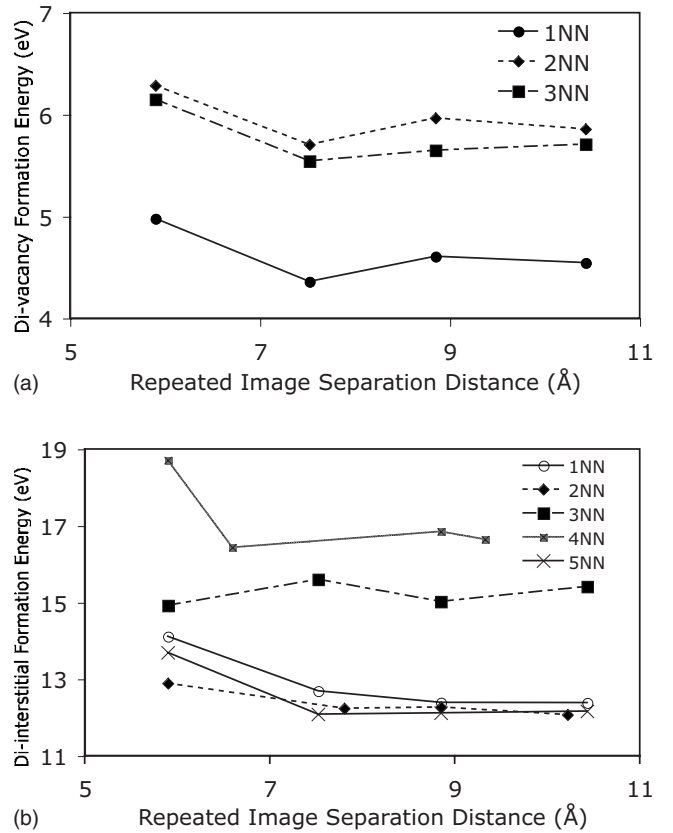

(a)

(b)

FIG. 4. Graphs that show the convergence of the formation energies as larger supercells are utilized. The energies in (a) are for Schottky defects and in (b) are for di-interstitials.

the Schottky defects by 1–3 eV, but underestimate the formation energies of the first, third, fourth, and fifth nearest neighbor di-interstitials by less than 1 eV.

Since the empirical potential calculations allow for many more atoms to be considered in the simulations, we continued the formation energy calculations for a variety of di-interstitials having larger separation distances. This allowed us to gain an insight into the point at which the isolated defect energy is reached. Figure 5 shows the formation energy of the di-interstitials as a function of the separation distance.

This graph shows that for a separation distance of larger than 7 Å, the formation energy lies close to 18 eV. This is in agreement with the converged value of 18.4 eV. For the larg-

TABLE III. The defect formation energies for the nearest neighbor Schottky defects and di-interstitials for both the DFT and the empirical potential calculations as a function of the defect separation.

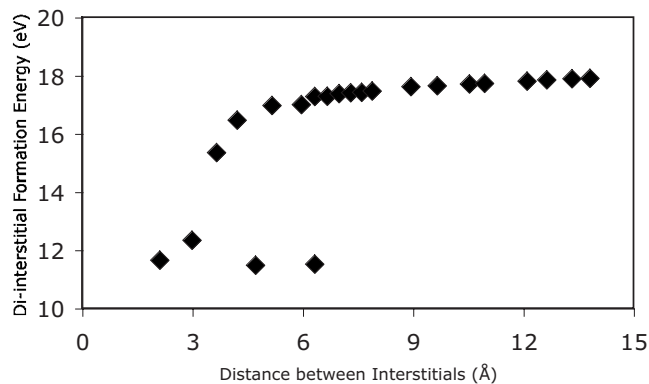| Defect separation	DFT formation energy (eV)		Emp. pot. formation energy (eV)	
	Schottky defect	Di-interstitial	Schottky defect	Di-interstitial
1NN	4.6	12.4	5.7	11.6
2NN	5.9	12.1	7.7	12.4
3NN	5.7	15.4	7.2	15.3
4NN		16.6		16.5
5NN		12.1		11.5

FIG. 5. Graph showing the formation energy of di-interstitials, calculated using empirical potentials, as a function of the separation between the two interstitial atoms.

est considered separation of interstitials (13–14 Å), the empirical potential predicts a formation energy of 17.9 eV. Also of interest is the fact that in addition to the first, second, and fifth nearest neighbor di-interstitials having a relatively low formation energy of 11.5–12.5 eV, another favorable configuration is predicted when the di-interstitials are in an eighth nearest neighbor configuration (separated by a distance of 6.32 Å), in a $\langle 221 \rangle$ direction. This has a formation energy of 11.5 eV. There exists another configuration with this same separation distance, but with the interstitials lying in a $\langle 100 \rangle$ direction, and this is predicted to have a much higher formation energy of 17.3 eV.

We studied the convergence of formation energies of Schottky defects in a similar manner, and the results of this analysis are presented in Fig. 6. Only a small deviation from the converged value of 8.8 eV occurs for separation distances greater than 6 Å.

In order to study these defects further, the relaxation of the structures and the defects was also analyzed. For the isolated defects, the directions of displacement of the atoms during the relaxation are shown in Fig. 7.

Table IV shows the magnitude of these displacements. It can be seen in this table, and in Fig. 7, that the surrounding Mg atoms are attracted toward a Mg vacancy, whereas the O
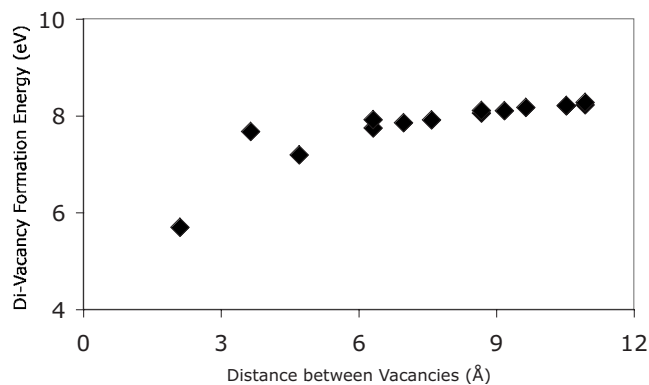

FIG. 6. Graph showing the formation energy of Schottky defects, calculated using empirical potentials, as a function of the separation between the two vacant lattice sites.
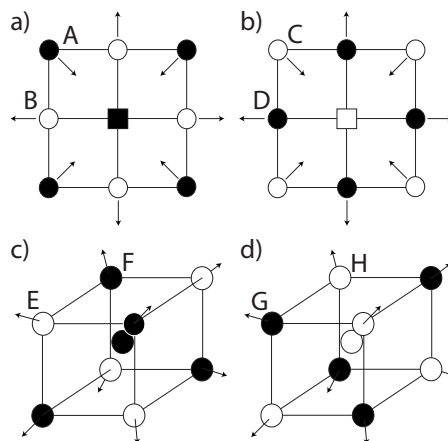

FIG. 7. The direction of displacement of the atoms surrounding the isolated defects: (a) Mg vacancy, (b) O vacancy, (c) Mg interstitial, and (d) O interstitial. The magnitudes of the displacements of selected atoms are shown in Table IV.

atoms are repelled. The opposite is true for the isolated interstitials. Directions of displacement are the same for both *ab initio* and classical potential calculations. Isolated interstitials cause atoms of the same species to move a greater distance than atoms of the other species. The DFT results show that the Mg displacement for the Mg interstitial is 0.45 Å compared to 0.023 Å for the O atoms and the O movement for the O interstitial is 0.48 Å compared to 0.017 Å for the Mg atoms. For the displacements of the atoms surrounding the isolated vacancies, the empirical potential simulation overestimates the magnitudes of the displacements by about 50%. The agreement between DFT and the empirical potentials is much stronger in the case of isolated interstitials, with less than 0.05 Å difference between the magnitudes of displacement predicted by the two computational methods. An earlier comparison between empirical potentials and *ab initio* calculations (GAMESS) was also given in Ref. 25. Although the relaxation distances calculated for atoms around the vacancies were similar, using the empirical

TABLE IV. The magnitude of the displacements of the atoms during relaxation by the DFT and the empirical potential methods. The labels refer to the letters in Fig. 7.

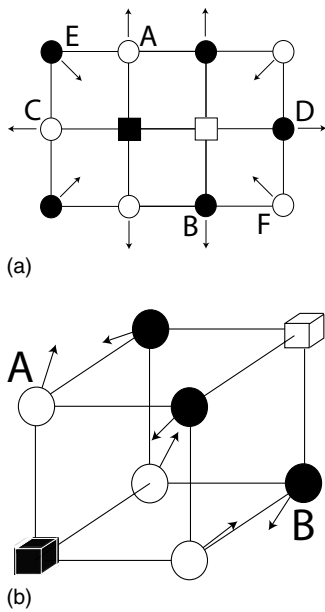| Defect	Label	DFT displacements (Å)	Empirical potential displacements (Å)
Mg vacancy	A	0.08	0.14
	B	0.12	0.21
O vacancy	C	0.07	0.11
	D	0.16	0.21
Mg interstitial	E	0.023	−0.023
	F	0.45	0.49
O interstitial	G	0.017	−0.024
	H	0.48	0.47

FIG. 8. The direction of displacement, during relaxation, of atoms surrounding the (a) first and (b) second nearest neighbor Schottky defects. Magnitudes of these displacements are given in Table V.

potentials, to those given here, the relaxation distances calculated using GAMESS were about double those from our *ab initio* results.

For the interacting defect pairs, a similar analysis was carried out. For the Schottky defects, the directions of displacements of atoms surrounding the first and second nearest neighbor Schottky defects are shown in Fig. 8, with the magnitudes for these displacements given in Table V.

It can be seen in Table V that the displacements surrounding the first nearest neighbor Schottky defect follow a trend similar to that of the isolated vacancies. Here, however, the magnitude of the oxygen displacement is predicted to be greater by the empirical potential simulations than the magnitudes calculated using DFT. This is also observed in the

TABLE V. The magnitude of the displacements of the atoms during relaxation of the first and second nearest neighbor Schottky defects by the DFT and the empirical potential methods. The labels refer to the letters for each on the atoms in Fig. 8.

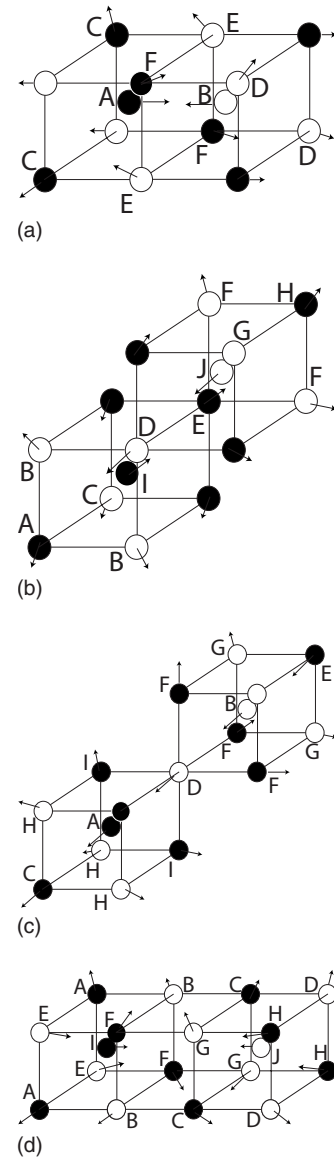| Defect	Label	DFT displacements (Å)	Empirical potential displacements (Å)
1NN Schottky defect	A	0.12	0.19
	B	0.17	0.18
	C	0.12	0.19
	D	0.16	0.18
	E	0.09	0.10
	F	0.09	0.10
2NN Schottky defect	A	0.13	0.20
	B	0.17	0.19

FIG. 9. The direction of displacement, from perfect lattice sites, of atoms surrounding the (a) first, (b) second, (c) third, and (d) fourth nearest neighbor di-interstitials. Magnitudes of these displacements are given in Table VI.

second nearest neighbor Schottky defect, with the empirical potential simulation overestimating the displacement of the O atoms by 54% but only overestimating the movement of surrounding Mg atoms by 12%. The third nearest neighbor Schottky defect follows a similar trend, in that the O atoms are predicted to move 35%–57% further than the DFT simulation shows. The displacements of the Mg atoms are again in good agreement, with only a 9%–11% overestimate by the empirical potentials.

Information about the atomic displacement of the di-interstitial configurations is shown in Fig. 9 and Table VI in the same way as for the Schottky defects. The first and fourth nearest neighbor di-interstitials are aligned in a ⟨100⟩ direction and the interstitial atoms remain an equidistance from the atoms at each of the cell sides but are attracted to each other. The second nearest neighbor and third nearest neigh-

TABLE VI. The magnitude of the displacements of the atoms during relaxation of the di-interstitial defects by DFT and empirical potential methods. The labels refer to letters in Fig. 9 and agreeing displacements of less than 0.3 Å are not shown.

Defect	Label	DFT displacements (Å)	Empirical potential displacements (Å)
1NN di-interstitial	C	0.42	0.43
	D	0.43	0.42
	E	0.58	0.54
	F	0.57	0.54
2NN di-interstitial	A	0.56	0.19
	B	0.56	0.41
	C	0.40	0.24
	D	1.72	0.80
	E	0.44	1.04
	F	0.16	0.41
	G	0.10	0.24
	I	0.13	0.58
	J	1.23	0.57
3NN di-interstitial	A	0.88	0.89
	B	0.45	0.39
	C	1.37	1.38
	D	0.87	0.88
	G	0.37	0.36
4NN di-interstitial	A	0.32	0.37
	D	0.34	0.35
	F	0.59	0.63
	G	0.58	0.62
	I	0.30	0.29
	J	0.29	0.31

bor configuration di-interstitials form split interstitials. In fact, the third nearest neighbor defect forms a crowdion along ⟨111⟩ consisting of four interstitial atoms along with two vacant sites.

With the exception of the second nearest neighbor di-interstitial, there is good agreement between the empirical potential simulation predictions and the DFT results. The differences in predicted magnitudes of displacement vary between methods by no more than 0.06 Å, with the majority of displacements agreeing to within 0.02 Å. The *ab initio*

method indicates that for the second nearest neighbor case, the Mg interstitial atom moves very little and it is only the O atom that should form a split interstitial with atom labeled D in the second nearest neighbor structure shown in Fig. 9. The empirical potential simulations predict that the Mg interstitial atom will form a second split interstitial with the Mg atom labeled E.

B. Transition energy barriers

An important factor when considering point defects in a material is the mobility of such a defect. It is of interest to know if it is likely that a defect can move freely within the material or whether it becomes trapped. Transition barrier energies are used to determine the likelihood of the system of atoms moving from one given configuration to another. This can therefore be used to analyze potential defect configuration changes, or simply a movement of the defect through the material. We have studied a variety of transition barriers using the nudged elastic band method.

Previous empirical potential calculations[2,5] indicate that interstitials are far more mobile than vacancies in MgO. We have looked at the possibility of a simple isolated vacancy migration and also considered the possibility of each of the three different Schottky defect configurations transforming into each other. We found that the isolated Mg vacancy has a migration barrier of 2.20 eV, whereas the O vacancy has a barrier of 2.31 eV. These values agree with those calculated using DFT by De Vita *et al.*[8] and using the semiempirical approach by Kotomin and Popov[23] who utilized the method of intermediate neglect of the differential overlap. Results from these sources were 2.39 and 2.43 eV, respectively, for the isolated Mg vacancy migration energy and 2.48 and 2.50 eV, respectively, for the isolated O vacancy migration energy.

Table VII shows transition energies for Schottky defect configuration changes. The six possible transitions between first, second, and third nearest neighbor Schottky defect configurations all have energy barriers greater than 1.3 eV. The two lowest barriers of 1.30 and 1.35 eV both correspond to transformations to the first nearest neighbor Schottky defect state (from third and second nearest neighbor configurations, respectively).

In considering the motion of an isolated interstitial atom, both Mg and O separately, we have studied a number of different mechanisms for the displacement of the isolated interstitial atom. The three possible directions considered were the ⟨100⟩-, ⟨110⟩-, and ⟨111⟩-type directions. Motion is possible through either a direct hop of an interstitial or an

TABLE VII. The transition energies of configuration changes of the Schottky defects studied.

Initial configuration	Final configuration		
	1NN Schottky defect	2NN Schottky defect	3NN Schottky defect
1NN Schottky defect		2.61	2.35
2NN Schottky defect	1.35		2.23
3NN Schottky defect	1.30	2.23	

TABLE VIII. The transition energies of the displacement of isolated magnesium and oxygen isolated interstitial atoms.

Transition mechanism	54 atom barrier (eV)		128 atom barrier (eV)	
	Magnesium	Oxygen	Magnesium	Oxygen
$\langle 100 \rangle$ direct hop	1.21	1.26	0.99	0.99
$\langle 110 \rangle$ direct hop	2.59	2.71		
$\langle 100 \rangle$ atom exchange	2.78	3.00		
$\langle 110 \rangle$ atom exchange	1.17	1.25	0.94	0.96
$\langle 111 \rangle$ atom exchange	0.83	0.59	0.71	0.44

exchange with a nearest neighbor atom of the same species, with the initial interstitial moving to occupy the lattice site of the neighboring atom, while the neighboring atom moves to become the interstitial in its new location. We first considered simplifying the calculations at the cost of accuracy in order to speed up the computations. Considering a 54 atom cell allowed us to see which of the transitions have the lowest energy. Following this, we then considered larger, 128 atom cells, in order to calculate these lowest energy barriers to a much higher degree of accuracy.

Table VIII shows the resulting energy barriers for isolated interstitial transitions, calculated using 54 atom cells. These values show that the $\langle 110 \rangle$ direct hop and $\langle 100 \rangle$ atom exchange are extremely unlikely, having energy barriers between 2.5 and 3 eV. Due to the fact that the $\langle 100 \rangle$ direct hop and $\langle 110 \rangle$, and $\langle 111 \rangle$ atom exchanges have much lower energy barriers ranging from 0.83 to no more than 1.26 eV, we studied these transitions using the larger 128 atom cell. The barrier energies computed using a 128 atom supercell were found to be between 0.1 and 0.3 eV smaller than those found using the 54 atom cells. The results are shown in Table VIII and indicate that the $\langle 111 \rangle$ atom exchange is the most likely transition to occur. Previous empirical potential simulations[24] have estimated a 0.32 eV energy barrier for the isolated Mg interstitial and 0.40 eV for the O interstitial, incorrectly indicating that motion of the Mg atom is the more favorable transition.

It is also of interest to study not only the displacement of interstitial atoms when they are isolated but also the displacement when the atom constitutes one-half of a di-interstitial. By considering displacements in this fashion, it allowed us to understand how di-interstitials move through the lattice. We computed the transition barriers for direct hops of the oxygen atom which would convert one di-interstitial configuration to another. Since we found the exchange mechanism to be favorable, we also computed the barriers for various exchanges of magnesium atoms. Magnesium atoms were considered in the exchanges because in the case of an isolated interstitial, for two of the three exchanges (in the $\langle 100 \rangle$ and $\langle 110 \rangle$ directions), the Mg atom exchange had a lower energy barrier than an O atom exchange.

Table IX shows the transition barriers that were calculated for various di-interstitial configuration changes. The table presents the configuration change, the mechanism for the transition, and the transition energy. These energies are approximately the same whether it is the Mg or O atom in the

di-interstitial that moves. If a mechanism does not appear in the table (e.g., 2NN-3NN exchange), it indicates that the transition occurs by passing through some intermediate phase first.

From these results, it is observed that from either the third or fourth nearest neighbor position, it is likely that the configuration will change such that the interstitial atoms become first nearest neighbors. The barriers for these transitions are 0.30 and 0.10 eV, respectively. Recalling that the first and second nearest neighbor di-interstitials were observed to have similar formation energies, it is important to note here that the 128 atom cell used here only produces an estimate to the actual formation energies shown in Table III. For example, the 128 atom cell predicts identical formation energies for first and second nearest neighbor di-interstitials. The transition energy for a first to second nearest neighbor transition, 0.74 eV, is therefore identical to that of a second to first nearest neighbor transition due to this approximation.

TABLE IX. The transition energies of configuration changes of the di-interstitials studied.

From	To	Mechanism	Barrier (eV)
1NN	2NN	Exchange (Mg)	0.74
1NN	2NN	Exchange (O)	0.51
1NN	2NN	Direct (O)	1.43
1NN	3NN	Exchange (Mg)	3.24
1NN	4NN	Direct (O)	4.36
1NN	5NN	Exchange (Mg)	1.48
2NN	1NN	Exchange (Mg)	0.74
2NN	1NN	Exchange (O)	0.51
2NN	1NN	Direct (O)	1.43
2NN	3NN	Direct (O)	6.05
3NN	1NN	Exchange (Mg)	0.30
3NN	2NN	Direct (O)	3.11
3NN	5NN	Exchange (Mg)	4.04
4NN	1NN	Direct (O)	0.10
5NN	1NN	Exchange (Mg)	1.48
5NN	3NN	Exchange (Mg)	6.98

The only exchange mechanism in a $\langle 111 \rangle$-type direction was that of a second to first nearest neighbor exchange. Due to the differences in migration energies of the isolated O and Mg interstitials, we also considered an O atom exchange mechanism for this transition and we found this to have a transition barrier of 0.51 eV (compared to the 0.74 eV for the Mg atom exchange). This was the only transition where there was a significant difference between the O and Mg movement.

Since the fifth nearest neighbor di-interstitial has a similarly low formation energy to the first and second nearest neighbor configurations, potential transitions between these states were investigated. The transition barrier between the fifth and first nearest neighbor was found to be 1.48 eV, which is relatively high, and we did not observe a single stage process between second and fifth nearest neighbors. The barriers to move from a third nearest neighbor to the much lower in energy second or fifth nearest neighbor state are surprisingly high (3.11 and 4.04 eV, respectively), with the only remaining single stage process being that of a transition to first nearest neighbor with a far lower barrier energy of 0.30 eV.

The results in Table IX show the single stage processes. Remaining transitions were all found to be multiple stage processes. Transitions from the fourth nearest neighbor configurations are observed to pass through the first nearest neighbor configuration (with an energy barrier of 0.10 eV) before they potentially form either a second or third nearest neighbor di-interstitial, with energy barriers of 0.74 or 3.24 eV, respectively. Our calculations indicate that the fifth nearest neighbor defect, both with a direct and an exchange mechanism, had to pass through multiple configurations to reach the fourth nearest neighbor state, which is unlikely given the large energy barrier required to reach the fourth nearest neighbor configuration.

An exchange mechanism was also observed in the empirical potential simulations for which a first nearest neighbor di-interstitial would move through the bulk material. Here, both the magnesium and oxygen atoms would exchange with atoms at the corner of their local cells and these displaced atoms would become the new interstitials. Empirical potential simulations predict a barrier energy of 0.75 eV (Ref. 24) for this displacement, whereas the *ab initio* simulations computed this energy to be 0.85 eV, which is in good agreement.

A Bader analysis was performed on the 128 atom cell, and this showed that in a perfect MgO lattice, the charge on a Mg atom is 1.83 and on an O atom is −1.83. The charges on atoms in the systems containing di-interstitials varied by no more than ±0.1 with charges on the actual interstitial atoms varying by this largest amount with the majority of the remaining atoms varying by no more that ±0.04. During the second to first nearest neighbor direct transition, the change in charge on the interstitial atom involved in the motion was negligible. We also calculated the charges on atoms in the systems containing single isolated vacancies. The results showed that charge was distributed throughout the atoms in the system rather than localizing on the vacant site.

IV. CONCLUSIONS

The Schottky defect formation energies predicted by empirical potential simulations were 1–3 eV larger than the energies calculated using DFT. The relaxed structures for these defects show that the empirical potential simulations overestimate the displacement of the surrounding oxygen atoms during relaxation. The most energetically favorable Schottky defect structure is the first nearest neighbor configuration, and this is apparent in both methodologies. The computation of transition barriers using DFT showed that Schottky defects were unlikely to change configuration; thus, it is likely that first nearest neighbor vacancies would be formed and would remain as such. The difference in the formation energy means that it is highly likely that empirical potential calculations are underestimating the number of defects formed.

Analysis of the di-interstitials showed that the formation energies generated from the empirical potential simulations differ from DFT results by less than 1 eV, with lower formation energies generally predicted by the empirical potential calculations. Unlike for the Schottky defects, the relaxed structures for these di-interstitial defects were in good agreement between simulation methodologies, both in terms of the directions and magnitudes of the displacements. This would account for the closer agreement between empirical potential and DFT formation energies of the di-interstitials. The only case where this is not true is the second nearest neighbor di-interstitial, where the formation energy was predicted to be 0.3 eV higher than that calculated using DFT, and the structure varied from that of the DFT result. The empirical potential simulation predicted that two split interstitials would form, whereas the DFT results show that only the oxygen atom forms a split interstitial. Both methodologies predicted the first, second, and fifth nearest neighbor di-interstitials to be the most energetically favorable of the studied di-interstitial defects. Empirical potential simulations also predict that there exists another low energy state in an eighth nearest neighbor configuration (this state has not been studied using *ab initio* methods).

The study of the transition barriers for the di-interstitials indicates that should a third or fourth nearest neighbor di-interstitial form, the very low energy barriers dictate that this would quickly form a first nearest neighbor di-interstitial in favor of the other defects studied. There is then a small chance that the configuration would switch between that of the first and second nearest neighbor di-interstitials. The barrier to move from a fifth nearest neighbor configuration appears to be quite high, and so it is expected that if a di-interstitial of this separation were to form, it would be unlikely to change configurations.

Isolated vacancies were found to have relatively high migration barriers of 2.20 and 2.31 eV for Mg and O vacancies, respectively, from the DFT calculations, thus to be practically immobile once formed. The DFT calculations predict much lower barriers for the isolated interstitials of 0.71 and 0.44 eV for an isolated Mg atom and O atom, respectively. The most favorable diffusion mechanism for the isolated interstitials was via an exchange with another atom of the same species in the $\langle 111 \rangle$ direction. Previous empirical potential simulations[24] have calculated a 0.32 eV energy barrier for the isolated Mg interstitial and 0.40 eV for the O interstitial. Thus, the *ab initio* calculations predict that the motion on the O sublattice will be much faster than that on the Mg sublat-

tice, in contrast to the empirical potential results, which will have a large effect on the way that defects are annealed after the collision cascade.

The Bader charge analysis showed that the atoms that surround defects have charges very similar to those in the bulk. Further, there is very little change in the charge during transitions; therefore, a fixed charge model appears to be an appropriate approximation to implement when utilizing empirical potentials.

The overall agreement between the two methodologies is reasonable, which indicates that the empirical potentials in the main give an acceptable description of MgO. The empirical potential employed performs well when describing interstitial-type defects but far less well when studying vacancies, where the description is poor. This also introduces errors into the calculations of the energies of the Frenkel defects. The use of the shell model makes the agreement better for the Frenkel defects, with the O Frenkel defect in good agreement but the formation energy of the Mg Frenkel defect still differs by 1.5 eV. The transition barriers for isolated interstitials, which dominate the annealing of the defects, are good for the migration of O interstitials but poor for the Mg interstitials. This has important implications for both how the annealing takes place and the time scale over which annealing would occur.

*Corresponding author. FAX: +44-15-09-223-969.

[1] E. A. Kotomin, P. W. M. Jacobs, N. E. Christensen, T. Brudevoll, M. M. Kaklja, and A. L. Dopov, Defect Diffus. Forum **143**, 1231 (1997).

[2] B. P. Uberuaga, R. Smith, A. R. Cleave, F. Montalenti, G. Henkelman, R. W. Grimes, A. F. Voter, and K. E. Sickafus, Phys. Rev. Lett. **92**, 115505 (2004).

[3] B. P. Uberuaga, R. Smith, A. R. Cleave, G. Henkelman, R. W. Grimes, A. F. Voter, and K. E. Sickafus, Phys. Rev. B **71**, 104102 (2005).

[4] G. Henkelman, B. P. Uberuaga, D. J. Harris, J. H. Harding, and N. L. Allan, Phys. Rev. B **72**, 115437 (2005).

[5] B. P. Uberuaga, R. Smith, A. R. Cleave, R. W. Grimes, A. F. Voter, and K. E. Sickafus, Nucl. Instrum. Methods Phys. Res. B **250**, 12 (2006).

[6] S. Y. Li, Z. L. Liu, Y. G. Nan, and Z. R. Zhang, Chin. J. Chem. Phys. **19**, 315 (2006).

[7] R. W. Grimes, C. R. A. Catlow, A. L. Shluger, R. Pandey, R. Baetzold, and A. H. Harker, *Defects in materials*, MRS Symposia Proceedings 209 (Materials Research Society, Pittsburgh, 1991), p. 257.

[8] A. De Vita, M. J. Gillan, J. S. Lin, M. C. Payne, I. Stich, and L. J. Clarke, Phys. Rev. Lett. **68**, 3319 (1992).

[9] A. De Vita, M. J. Gillan, J. S. Lin, M. C. Payne, I. Stich, and L. J. Clarke, Phys. Rev. B **46**, 12964 (1992).

[10] D. Alfe and M. J. Gillan, Phys. Rev. B **71**, 220101(R) (2005).

[11] S. D. Kenny, A. P. Horsfield, and H. Fujitani, Phys. Rev. B **62**, 4899 (2000).

[12] P. Hohenberg and W. Kohn, Phys. Rev. **136**, B864 (1964).

[13] W. Kohn and L. J. Sham, Phys. Rev. **140**, A1133 (1965).

[14] C. Hartwigsen, S. Goedecker, and J. Hutter, Phys. Rev. B **58**, 3641 (1998).

[15] S. Goedecker, M. Teter, and J. Hutter, Phys. Rev. B **54**, 1703 (1996).

[16] H. J. Monkhorst and J. D. Pack, Phys. Rev. B **13**, 5188 (1976).

[17] R. W. G. Wyckoff, *Crystal Structures* (Wiley, New York and London, 1964).

[18] M. J. L. Sangster, G. Peckham, and D. H. Saunderson, J. Phys. C **3**, 1026 (1970).

[19] G. V. Lewis and C. R. A. Catlow, J. Phys. C **18**, 1149 (1985).

[20] V. R. Saunders, R. Dovesi, C. Roetti, R. Orlando, C. M. Zicovich-Wilson, N. M. Harrison, K. Doll, B. Civalleri, I. Bush, and P. D'Arco, *CRYSTAL2003 User's Manual* (University of Torino, Torino, 2003).

[21] G. Henkelman and H. Jónsson, J. Chem. Phys. **113**, 9978 (2000).

[22] E. Sanville, S. D. Kenny, R. Smith, and G. Henkelman, J. Comput. Chem. **28**, 899 (2007).

[23] E. A. Kotomin and A. I. Popov, Nucl. Instrum. Methods Phys. Res. B **141**, 1 (1998).

[24] B. P. Uberuaga, R. Smith, A. R. Cleave, G. Henkelman, R. W. Grimes, A. F. Voter, and K. E. Sickafus, Nucl. Instrum. Methods Phys. Res. B **228**, 260 (2005).

[25] R. W. Grimes, C. R. A. Catlow, and A. M. Stoneham, J. Phys.: Condens. Matter **1**, 7367 (1989).